SUPPLEMENTARY INFORMATION:

Autonomous bacterial localization and gene expression based on nearby cell receptor density

Table of Contents

Text

I. Creating a library of engineered bacterial strains with different AI-2 sensitivity

II. Evaluating expression and capability of protein G surface display

III. Demonstration of AI-2 mediated *E. coli* W3110 chemotaxis

IV. *In vitro* model to evaluate targeting selectivity through W3110 chemotaxis

i. Bacterial AI-2 chemotaxis study with AI-2 concentration gradient generated in a microfluidic device

ii. W3110 targeting in transwells with PCI-15B

Figures

Supplementary Figure 1. Sensitivity of strains engineered for altered response to AI-2

Supplementary Figure 2. Outer membrane protein G expression

Supplementary Figure 3. Effect of AI-2 on W3110 (Δ*lsrFG* Δ*luxS*) motility

Supplementary Figure 4. W3110 (Δ*lsrFG* Δ*luxS*) chemotaxis in microfluidic device

Supplementary Figure 5. Selectivity of functional dirigible system in transwell configuration

Supplementary Figure 6. Raw images of Supplementary Fig. 5.

I. Creating the library of engineered bacterial strains with different AI-2 sensitivity

Quorum sensing (QS) is a microbial cell-to-cell communication process mediated through secreted signaling molecules that coordinate unicellular properties, guiding multicellular behavior (Hooshangi & Bentley, 2008; March & Bentley, 2004). Among various signaling molecules, autoinducer-2 (AI-2) is synthesized by over 80 species and has been referred to as the "universal" QS signal molecule (Wang et al, 2005; Xavier & Bassler, 2005). AI-2 production is mediated by two enzymes: Pfs and LuxS. Initially, AI-2 accumulates extracellularly and then is imported back into cells by the Lsr ABC-type transporter when cell density reaches a putative threshold, or "quorum". Intracellular AI-2 is then phosphorylated by kinase LsrK and the resultant phospho-AI-2 activates further expression of Lsr components, in part, by binding transcriptional regulator LsrR. Phospho-AI-2 is then metabolized by LsrF/LsrG. This combined negative and positive regulatory structure of AI-2 mediated QS results in the tight regulation of the multicellular switch (Hooshangi & Bentley, 2011).

In order to tune the AI-2 responsiveness of *E. coli*, using our model we identified changes in genes and regulatory functions that would putatively alter the genetic response of the bacteria to AI-2. Then, we created a small library of *E. coli* W3110 mutants by rewiring the transduction pathway. We created a *luxS* and *lsrFG* double knockout (CT104) using phage_Red recombination (Datsenko & Wanner, 2000). We also constructed plasmids to express either the kinase, LsrK, or the entire ABC-type transporter consisting of genes *lsr* ACDB under the pBAD promoter (Guzman et al, 1995) in order to enhance AI-2 uptake and phosphorylation. These were transformed into MDAI2 bacteria (W3110 Δ*luxS*) so that only *in vitro* synthesized AI-2 would trigger a response. We also transformed the pCT6/pET-DsRed plasmids (Tsao et al, 2010) into all strains to provide DsRed expression in response to AI-2. During experiments, all bacteria were grown in LB media at 37^{o}C and 250rpm. Unless otherwise noted, they were supplied with various amounts of *in vitro* synthesized AI-2 (Fernandes & Bentley, 2009). After an 8 hr incubation, bacterial responses were measured via flow cytometry. As shown in **Supplementary Fig. 1**, CT104 (Δ*lsrFG* Δ*luxS*) showed the most sensitive response to AI-2 (initial DsRed appeared with < 1μM AI-2 and reached 50% of the population at 5μM AI-2). The strains containing overexpressed LsrK and the Lsr ACDB were also more sensitive than the wild type control strain MDAI2, (W3110 Δ*luxS*). Additionally (not shown) we created *lsrR luxS* and *lsrK luxS* double mutant strains which also had an altered AI-2 sensitivity compared to the wild type

strain (Hooshangi & Bentley, 2011). Therefore, we demonstrate that this system can be tuned by selecting dirigible cells from a library of AI-2 responding strains that have altered AI-2 sensitivity.

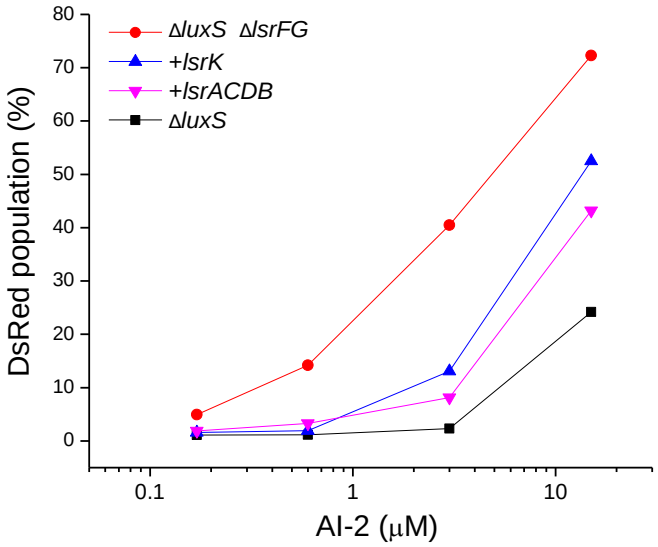

Supplementary Figure 1 Sensitivity of strains engineered for altered response to AI-2. Bacteria were induced with various amounts of *in vitro* synthesized AI-2 and incubated for 8 hr. Subsequently, cells were harvested and DsRed positive cells were reported as a fraction of the total after flow cytometry.

II. Evaluating expression and capability of protein G surface display

In order to enable surface "docking" capability, we surface expressed an ompA-protein G fusion on host cells. By subsequent incubation with a surface-specific antibody, we assembled docking antibodies onto the outer surface of *E. coli*. This generic platform enabled the binding of bacterial cells to avidin and EGFR on surfaces of chips or mammalian cells. We adopted the surface display strategy from Georgiou (Francisco et al, 1992) which utilizes outer membrane protein A (*ompA*) to exhibit protein G (Tanaka et al, 2006). We incorporated the protein G motif into the pET-DsRed vector, as described previously, to generate the plasmid pET-DsRed_tac-ompAG1 where *ompAG1* is placed under ptac promoter control. The resultant vectors (**Supplementary Fig. 2A**) were co-transformed into CT104. The subsequent strain was capable of expressing protein G in response to IPTG and DsRed in the presence of AI-2. **Supplementary Fig. 2B** depicts the expression profile induced by varied concentrations of IPTG. Bacteria were induced by varied concentrations of IPTG (0, 0.05, 0.1, and 0.5mM). After

1.5~2hr induction at 37°C 250 rpm shaking, the relative expression levels of protein G on the outer surface were quantified. Visualization is afforded by DL488 labeled anti-mouse IgG staining; protein G expression level was titrated via both fluorescence images and flow cytometry. The fact that the DL488 fluorescence intensities increased with the concentration of IPTG indicates increased expression of protein G, with minimal alteration of DsRed (near zero, **Supplementary Fig. 2B**). The expression of surface displayed protein G enables titration of avidity to the targets of interest.

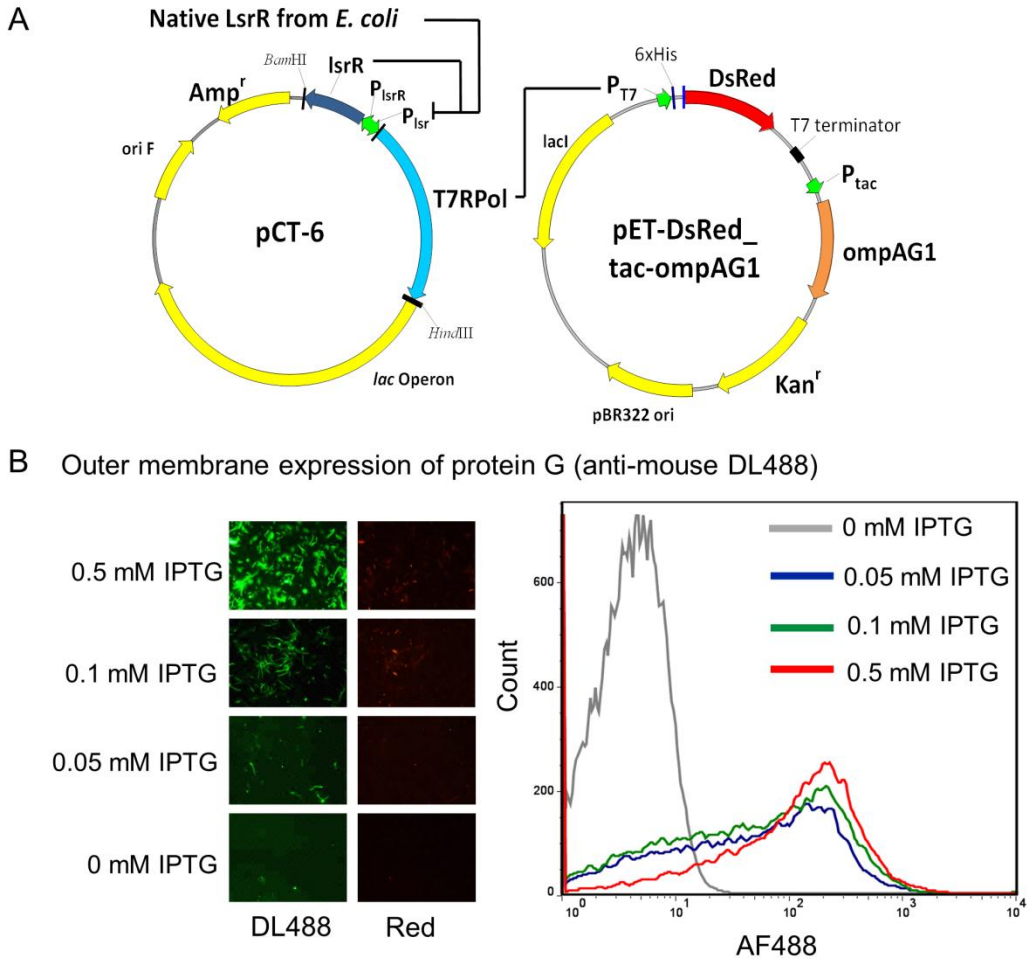

Supplementary Figure 2 Outer membrane protein G expression. (A) Schematic of the pCT6 + pET-DsRed_tac-ompAG1 vector sets. The vectors were transformed into CT104 (W3110 Δ*lsrFG* Δ*luxS*) for expression. (B) Protein G expression profile was determined by inducing with varied concentrations of IPTG. After 1.5~2hr induction, the relative expression levels of protein G on bacterial outer surfaces were quantified. Through visualization afforded by DL488 labeled anti-mouse IgG staining, the protein G expression level was titrated via fluorescence images and flow cytometry.

III. Demonstration of AI-2 mediated *E. coli* W3110 chemotaxis

To study the effects of AI-2 on bacterial motility, we performed a series of experiments using the transwell apparatus, commonly used for eukaryotic cells, to track bacterial migration. Briefly, we applied AI-2 in the top transwell and bacteria in the bottom well and then calculated the amount of bacteria that had travelled to the top well by measuring optical density (OD_{600}). First, as controls we investigated the role of several buffer solutions and chemicals that bacteria would potentially encounter throughout this set of experiments. Concentrations of solutions indicated were all adjusted to 40μM (in DPBS) and added to the top wells. Bacteria were incubated at 37^{o}C in a static condition for two hours followed by OD measurement. In **Supplementary Fig. 3A**, the AI-2-containing well showed the highest bacterial OD, indicating the most significant chemoattraction occurred when exposed to AI-2. Other wells provided with either DPBS, Tris-HCl, homocysteine (a by-product of AI-2 synthesis), and S-adenosylhomocysteine (SAH, precursor of AI-2) showed very low OD. These indicate that AI-2 was a positive chemoattractant for *E. coli W3110* (Δ*lsrFG* Δ*luxS*) from among our tested compounds. We conducted additional experiments to quantitatively investigate sensitivity to AI-2. That is, we tested for a dose-dependent of AI-2 on motility. Using varied concentrations of AI-2 in DPBS, we performed analogous experiments, measuring OD in the two chambers 1 and 2 hrs post-incubation.As depicted in **Supplementary Fig. 3B**, the OD increased initially at AI-2 below 1μM for the two-hour curve, reaching a plateau at ~5-10μM. Interestingly, there was little change in OD for all the 1 hr samples, indicating minimal motility at all concentrations. We estimated the typical migration distance to be 3.5 mm, which when combined to the time associated with initiating accelerated swimming, precluded significant movement to the upper chamber. Overall, these results indicate a concentration threshold of AI-2 and an appropriate response time needed for attracting bacteria in this experimental setup.

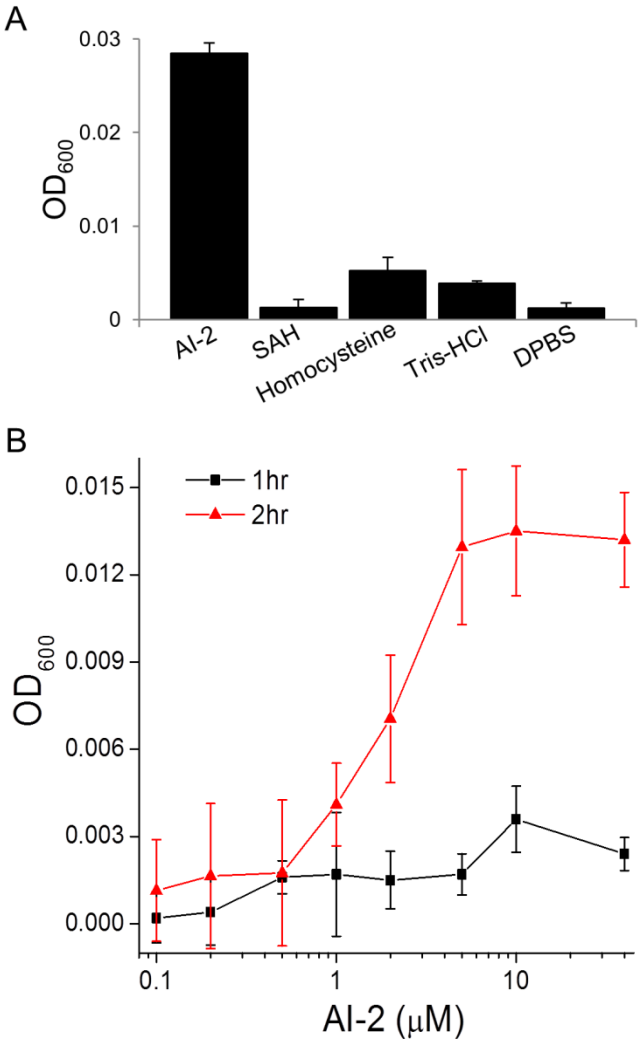

Supplementary Figure 3 Effect of AI-2 on CT104 motility. (A) Determination of AI-2 as a chemoattractant. Equivalent molar concentration (40μM) of AI-2, SAH (precursor of AI-2), homocysteine (side product of *in vitro* AI-2 synthesis), and buffer (DPBS, Tris-HCl) were tested as chemoattractants. (B) Dosage dependent AI-2 chemotaxis. Various concentrations of AI-2 were prepared and tested for bacteria motility. OD measurements in the upper chamber were performed at one and two-hour post-incubation.

IV. W3110 chemotaxis: Initial characterization of spatial and temporal resolution

While the successful performance of the engineered bacteria has been demonstrated *in vitro* in the main text, the function and degree of success might be potentially compromised in a more realistic scenario, i.e. in an *in vivo* model, due to the dynamics of the tumor microenvironments (Sun et al, 2012). The complexity of tumor geometry, vascularization, diffusion barriers, etc., are the often causes for the deficiency of cancer therapeutics (Cairns et al, 2006; Casanovas, 2012; Sun et al, 2012), and would likely affect design of the dirigible system.

That is, bacterial motility and targeting here are governed by AI-2 diffusion so that with respect to tumor geometry, targeting specificity is a concern. We have carried out a series of experiments that attempt to shed light on spatial resolution of bacterial migration. That is, could this system as it is currently assembled differentiate one cell from a directly adjacent cell with different marker density? This question seeks basic information as to diffusion and migration length and time scales. We devised two experimental setups to provide initial characterization of these phenomena: (i) a microfluidic chamber was constructed in which bacteria were exposed to a well-defined AI-2 gradient; and (ii) the transwell apparatus shown above and in the main manuscript was modified to explore length and time limits for spatial resolution of cell populations.

IV. i. Bacterial AI-2 chemotaxis with AI-2 concentration gradients generated in a microfluidic device

We designed a microfluidic system for generating stable chemical gradients through controlled diffusion in order to monitor bacterial migration (Ahmed et al, 2010; Diao et al, 2006). In **Supplementary Fig. 4A**, this device consists of three channels aligned in parallel. The middle channel, 2 mm wide, served as the main chamber for observing cell migration with an inlet and outlet allowing the introduction and exit of bacterial populations. Two side channels, each 500 μm wide, served as either a source or sink of AI-2. The channels were connected by arrays of smaller perpendicular channels (100 μm wide, spaced at 100 μm) that enabled diffusion of molecular species while minimizing convective flux (Ahmed et al, 2010; Diao et al, 2006) . This configuration enables stable and static concentration gradients within the middle main channel by diffusional transport between the two outer channels. The microfluidic device consists of a

top poly(dimethylsiloxane) (PDMS) cover and bottom glass slide. The top PDMS cover was replicated from a SU-8 mold fabricated using standard photolithography techniques on a silicon wafer. After punching holes for the inlets and outlet with a puncher, the PDMS cover was oxygen plasma treated to irreversibly bond to the glass slide.

The generated gradient was calibrated using 0.1 mM fluorescein (Sigma) and 0.1mM DPBS buffer (**Supplementary Fig. 4B**). A well-defined linear gradient in the middle regime of the main chamber can be seen by plotting the integrated fluorescence intensity profile over the main chamber (**Supplementary Fig. 4B**). The flow rate for both side channels was 2.0 µl/min. The inlet and outlet of the main chamber was blocked to maintain a static condition.

To observe and evaluate bacterial chemotaxis, we introduced populations of bacteria (OD_{600} =2.0) to the main chamber, then sealed the inlet and outlet of the chamber. The bacteria used here constitutively express red fluorescent proteins for rapid and simple visualization and tracking by fluorescence microscopy. That is, plasmid pQE60-T5-DsRed-Express2 (Strack et al, 2008), which allows for constitutive DsRed expression, was transformed into CT104 to facilitate the observation. Based on our results using the transwell apparatus, we hypothesized that the bacteria might respond quickly as well as correlate positively to the well-defined AI-2 chemical gradient (see **Supplementary Fig. 4C**). Specifically, both side channels were perfused with DPBS buffer at a flow rate of 2.0 µl/min. The cells, which were preloaded, did not distribute in a preferred directionality during the 30 min duration (left image of **Supplementary Fig. 4D**). The fluid perfused through the leftmost channel was then replaced with 30 µM AI-2 at the same flow rate. The cell distribution was imaged again after ~30-40 min. Migration of CT104 towards AI-2 was readily observed upon generation of the imposed AI-2 concentration gradient (~0.06 mM/mm), which led to a biased cell distribution with a significant number of bacteria gathering in the high concentration zone (right image of **Supplementary Fig. 4D**). We note that the assembly of the gradient without cells takes < 4 min upon introduction of the chemoattractant fluid in the leftmost channel.

These results reinforce our observations that W3110 migrate towards regions of higher AI-2 concentration when provided unobstructed pathways to defined locales within a sub-millimeter range.

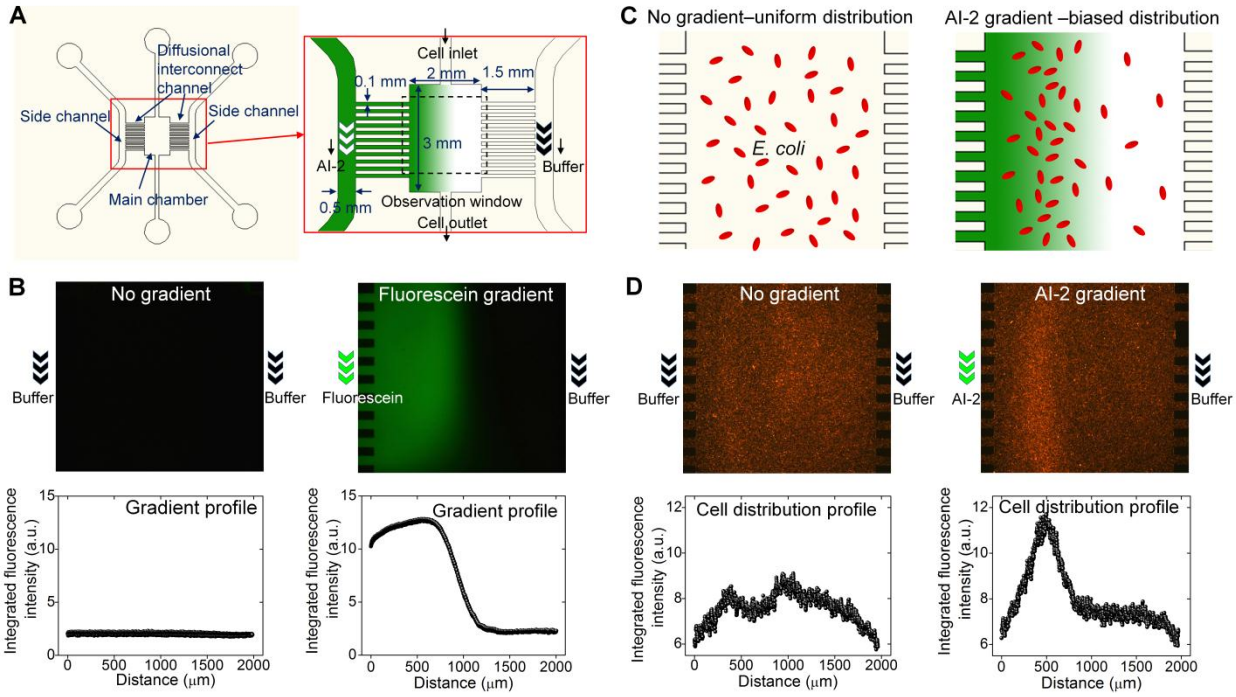

Supplementary Figure 4. CT104 chemotaxis in a microfluidic device. (A) Schematic diagram of the microfluidic design. The device is capable of generating a stable and static chemical concentration gradient in the central chamber by diffusion from two side channels. (B) Calibration of the generated gradient using fluorescein and PBS buffer solutions. Figures on the left: Fluorescence micrograph and gradient profile of the main chamber when there was no concentration gradient (both side channels were filled with PBS buffer solution). Figures on the right: Fluorescence micrograph and gradient profile of the main chamber when there was a concentration gradient of fluorescein (the left and right side channels are filled with fluorescein and PBS respectively). (C) Schematic diagrams of the bacterial distribution profile in the main chamber with and without a device-imposed concentration gradient of AI-2. Bacteria migrate toward higher AI-2 concentrations. (D) Fluorescence micrograph and cell distribution profile of the main chamber when populations of bacteria were introduced to no gradient (left) and gradient of AI-2(right).

IV. ii. W3110 targeting in transwells with PCI-15B

In order to further explore targeting selectivity and motility of the functioning programmed dirigible system, we performed a series of experiments using the transwell configuration.

Specifically, we cut the glass slide (22mm round; Fisher Scientific) into two roughly identical halves, treated each half with gelatin, and seeded each with the same number of PCI-15B cells one day prior to experiments. One half was then treated with anti-EGFR+NF, representing the cancer target loaded at a high NF density, while the other half was treated with anti-EGFR, representing the healthy cell at low NF density. We then aligned the two half slides together and placed them upside-down into 500μM SAH (DPBS) containing transwells (3μm porosity; 6 well plate formats). Alignment of both slides at a distance of 1-2 mm provides an initial test of spatial resolution. CT104 carrying pQE60-T5-DsRed-Express2 (above) was added to the into the bottom compartment (OD_{600} ~0.05 in DPBS) and incubated at 37^{o}C (in 5% CO_2) for 3.5 hours. The bacterial motility and selectivity were determined by examining the amount of DsRed bacteria bound on the slides using fluorescence microscopy. Results depicted in **Supplementary Fig. 5** are based on the image analyses of the respective raw images taken from **Supplementary Fig. 6**.

In the schematic of **Supplementary Fig. 5A**, blue designates cells without NF while green designates cells with NF. The binding of DsRed bacteria (determined by image analyses, Image J) indicates that similar numbers of bacteria bound to both slides irrespective of the presence of the NF. This indicates that the bacteria were not able to distinguish the desired target from the control given the 1-2 mm separation. Note, at time zero SAH and bacteria were introduced so the concentration gradient (which is not well characterized here) is established and dissipated within the 3.5 hr window. The result clearly demonstrates that directionality of the AI-2 gradient and subsequent cell migration will impact resolution. That is, the AI-2 molecules locally synthesized from the NF (green) surface radiated out isotropically across the membrane as well as the non-NF (blue) surface within the diffusible range (~1-2 mm in 3.5 hrs) (Hille, 2001; Truskey et al, 2004), resulting in non-specific targeting of bacteria (the right figure of **Supplementary Fig. 5A**). We note that in the microfluidic device (**Supplementary Fig. 4 B**), the distribution of small molecules was maintained steady and therefore the gradient remained spatially well-defined even within the scale of 1mm in distance (100% on left and 0% on right). In this situation, the bacteria were able to recognize the differences in AI-2 concentration and migrated towards the high concentration in a uniform manner. These results demonstrate collectively, that the bacteria were capable of selectively migrating when AI-2 gradient was spatially well-distributed. Once the motility was actuated by the cells upon sensing AI-2 above

its threshold, they migrated toward the AI-2 laden locales. Thus, the closer the distance between the targeted (NF-bound) to the non-targeted (non NF-bound) locales, the higher the chance that AI-2 will bleed over the entire region and causing the less specific migration and docking of bacteria.

We then performed another two sets of experiments by scaling up the dimension from the 6-well plate system to a petri-dish configuration so that greater length scales could be examined. Similar to **Supplementary Fig. 5A**, PCI-15B cells were seeded on two slides (12 mm round; poly-D-lysine treated; BD Biosciences), independently decorated with anti-EGFR+NF (green) and anti-EGFR only (blue), and subsequently placed up-side-down into the transwells. As indicated in the schematic of **Supplementary Fig. 5B**, the slides were located into 6-well transwells which were placed into a 100mm petri-dish containing ~0.01 OD of bacteria CT104 (pQE60-T5-DsRed-Express2). This experimental set-up is actually complementary to Fig. 5A.. The results clearly indicate preferential motility of bacteria toward the desired slide (green; with NF treated). We also observed that preferential migration occurred at this length scale over a 1.5 to 2.5 hr period. From the control experiment results, there was no apparent bleeding of AI-2 from the test sample obscuring migration to non-targeted locales. The length scale tested in this setup is far beyond accessible for simple diffusion of AI-2 within the experimental time frame. That is, the actual distance between the edges of both slides (green vs. blue) is around 40mm and the diffusion time for AI-2 to travel horizontally from the NF to the non-NF transwell is roughly estimated to be about 370 hours (Hille, 2001; Truskey et al, 2004). This suggests that the non-NF transwell (blue) remains without AI-2 contamination during the experimental time window (2.5 hours). In parallel to **Supplementary Fig. 5B**, we performed an experiment wherein the cross diffusion of AI-2 between locales was not inhibited by the transwells. That is, AI-2 generated at a surface could isotropically diffuse generating an attractant gradient experienced by many cells in a distributed environment. This then provides an extreme length scale to test migration specificity. Specifically, the PCI-15B cells were prepared and treated with the same procedures above: NF decorated (green) and without NF anchored (blue). Both slides were incubated directly into the same petri-dish transwell (Corning; 75mm diameter, 3μm porosity) but placed at a 50mm spacing to mimic a situation where two distant spots are tested (e.g., between cancerous and healthy tissues., schematic of **Supplementary Fig. 5C)**. The same bacteria (~0.01 OD; CT104 with pQE60-T5-DsRed-Express2) were then introduced to the bottom petri-dish followed

by incubation at 37^{o}C (in 5% CO_2). As shown in the right panelof **Supplementary Fig. 5C**, the bacteria were found more preferentially on the NF-loaded cells (green spots) and not on either control. Moreover, the results were unchanged between 1.5 and 2.5 hr. This result provides additional evidence that bacterial targeting within the range of a centimeter length scale is entirely feasible given the concentrations, cells, and time scales tested here.

Overall, the results from **Supplementary Fig. 4** and **5** provide evidence that spatial localization of AI-2 synthesizing nanofactories can be resolved by bacteria that migrate towards targeted locations when they recognize the synthesized chemotactic gradient. Our data also reinforce the concept that AI-2 concentration, as assembled either enzymatically, by flow, or perhaps by other bacteria, could lead to migration and threshold-based actuation of gene expression. Importantly, our data suggest that relatively small gradients in AI-2 applied for short time durations are all that is needed to direct bacterial migration. Moreover, our data suggest that the direction of the AI-2 gradient and the relative migration path of the bacteria need to be considered in parallel. That is, at long length scales selective migration of bacteria is enabled irrespective of the directionality of AI-2 generation. Cells will find the highest concentration and seek it out. At short length scales (~mm), in order for bacteria to migrate in a selective manner, the AI-2 gradient and the migration path must be aligned. Perhaps most importantly, the system shown here reveals features of time and length scale (e.g., small molecule diffusion, bacterial migration, etc.) that should be considered further for accurate design and implementation of a disease-specific or application-specific treatment.

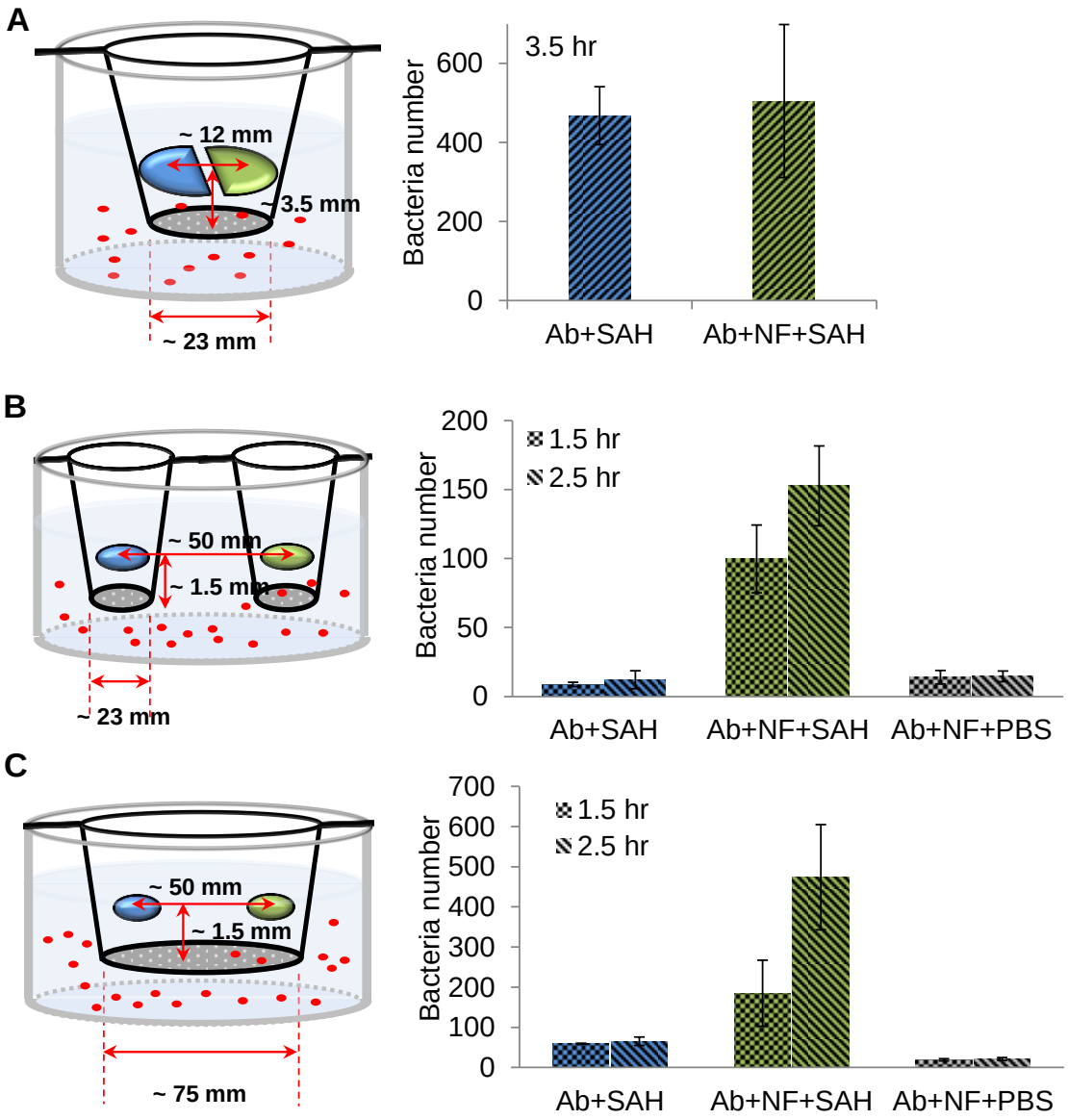

Supplementary Figure 5. Targeting selectivity of CT104 in presence of PCI-15B. (A) Bacteria chemotactic migration and targeting toward two closely aligned samples. The schematic shown in the left figure: PCI-15B cells were seeded into two identical half round glass slides pre-treated with gelatin and then decorated with anti-EGFR+NF (designated as green) and anti-EGFR only (designated as blue). Both slides were placed up-side down and aligned adjacently (~1-2mm separation) in the same 6-well transwell filled with SAH (in DPBS buffer). CT104 (pQE60-T5-DsRed-Express2) were added to the bottom of the wells (OD ~0.05) and after 3.5 hours at 37^{o}C, fluorescence images of the slides were taken. The targeting results are shown at the right. (B) Bacterial motility and targeting toward two distant samples within a confined environment. The schematic diagram on the left represents the configuration. Both transwells were placed in a 100 mm petri-dish, followed by addition of bacteria (OD ~0.01). The green slide is designated anti-EGFR+NF+SAH; blue is anti-EGFR+SAH. Another PCI-15B seeded slide was treated with anti-EGFR+NF and placed into another transwell containing only DPBS, which served as a negative control (designated gray). The results of targeting are depicted in the rightmost figure. (C)

Bacterial motility and specific targeting toward two distant samples within a spatially unrestricted environment. As indicated in the schematic on the left, the configuration of both anti-EGFR+NF+SAH (green slide) and anti-EGFR+SAH (blue slide) were both placed in the same transwell (petri-dish size; 100mm) where, unlike 5B, there was no restriction to diffusion between the two locations. Bacteria (OD ~0.01) were added into the bottom petri-dish at time zero. The resultant selectivity was shown in the right figure. All of the raw fluorescence images for the analytical plots in this figure are shown in **Supplementary Fig. 6**.

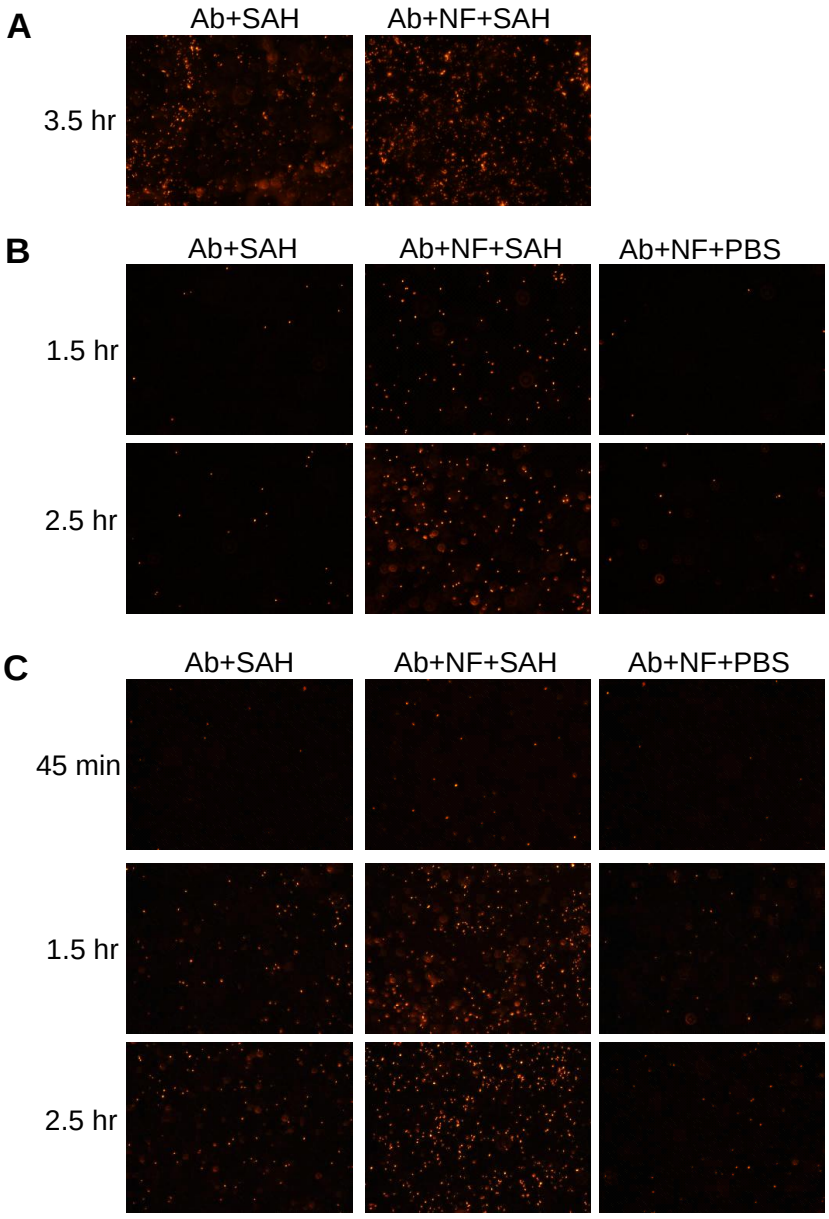

Supplementary Figure 6. Raw images for motility experiments of Figure 5. (A) Bacteria chemotactic migration and targeting toward two closely aligned samples. (B) Bacteria motility and specific targeting toward two distant samples in a confined environment. (C) Bacteria motility and specific targeting toward two distant samples within a free environment.

Supplementary references

Ahmed T, Shimizu TS, Stocker R (2010) Bacterial chemotaxis in linear and nonlinear steady microfluidic gradients. *Nano letters* **10:** 3379-3385

Cairns R, Papandreou I, Denko N (2006) Overcoming physiologic barriers to cancer treatment by molecularly targeting the tumor microenvironment. *Molecular cancer research : MCR* **4:** 61-70

Casanovas O (2012) Cancer: Limitations of therapies exposed. *Nature* **484:** 44-46

Datsenko KA, Wanner BL (2000) One-step inactivation of chromosomal genes in Escherichia coli K-12 using PCR products. *Proceedings of the National Academy of Sciences of the United States of America* **97:** 6640-6645

Diao J, Young L, Kim S, Fogarty EA, Heilman SM, Zhou P, Shuler ML, Wu M, DeLisa MP (2006) A three-channel microfluidic device for generating static linear gradients and its application to the quantitative analysis of bacterial chemotaxis. *Lab on a chip* **6:** 381-388

Fernandes R, Bentley WE (2009) AI-2 biosynthesis module in a magnetic nanofactory alters bacterial response via localized synthesis and delivery. *Biotechnol Bioeng* **102:** 390-399

Francisco JA, Earhart CF, Georgiou G (1992) Transport and anchoring of beta-lactamase to the external surface of Escherichia coli. *Proceedings of the National Academy of Sciences of the United States of America* **89:** 2713-2717

Guzman LM, Belin D, Carson MJ, Beckwith J (1995) Tight regulation, modulation, and high-level expression by vectors containing the arabinose PBAD promoter. *J Bacteriol* **177:** 4121-4130

Hille B (2001) *Ion Channels of Excitable Membranes*, 3rd edn. Sunderland: Sinauer Associates, Inc.

Hooshangi S, Bentley WE (2008) From unicellular properties to multicellular behavior: bacteria quorum sensing circuitry and applications. *Current opinion in biotechnology* **19:** 550-555

Hooshangi S, Bentley WE (2011) LsrR quorum sensing "switch" is revealed by a bottom-up approach. *PLoS Comput Biol* **7:** e1002172

March JC, Bentley WE (2004) Quorum sensing and bacterial cross-talk in biotechnology. *Current opinion in biotechnology* **15:** 495-502

Strack RL, Strongin DE, Bhattacharyya D, Tao W, Berman A, Broxmeyer HE, Keenan RJ, Glick BS (2008) A noncytotoxic DsRed variant for whole-cell labeling. *Nature methods* **5:** 955-957

Sun Y, Campisi J, Higano C, Beer TM, Porter P, Coleman I, True L, Nelson PS (2012) Treatment-induced damage to the tumor microenvironment promotes prostate cancer therapy resistance through WNT16B. *Nature medicine* **18:** 1359-1368

Tanaka G, Funabashi H, Mie M, Kobatake E (2006) Fabrication of an antibody microwell array with self-adhering antibody binding protein. *Analytical biochemistry* **350:** 298-303

Truskey GA, Yuan F, Katz DF (2004) *Transport Phenomena in Biological Systems*, 1st edn. Upper Saddle River, New Jersey: Pearson Education, Inc.

Tsao CY, Hooshangi S, Wu HC, Valdes JJ, Bentley WE (2010) Autonomous induction of recombinant proteins by minimally rewiring native quorum sensing regulon of E. coli. *Metab Eng* **12:** 291-297

Wang L, Hashimoto Y, Tsao CY, Valdes JJ, Bentley WE (2005) Cyclic AMP (cAMP) and cAMP receptor protein influence both synthesis and uptake of extracellular autoinducer 2 in Escherichia coli. *J Bacteriol* **187:** 2066-2076

Xavier KB, Bassler BL (2005) Regulation of uptake and processing of the quorum-sensing autoinducer AI-2 in Escherichia coli. *J Bacteriol* **187:** 238-248